Thermal and thermo-mechanical solution of laminated composite beam based on a variables separation for arbitrary volume heat source locations

Philippe Vidal, Laurent Gallimard, Isabelle Ranc, Olivier Polit

Thermal and thermo-mechanical solution of laminated composite beam based on a variables separation for arbitrary volume heat source locations

P. Vidal*, L. Gallimard, I. Ranc, O. Polit

UPL, Univ Paris Nanterre, Laboratoire Energétique, Mécanique, Electromagnétisme, 50 rue de Sèvres - Ville d'Avray, 92410 France

A B S T R A C T

In this work, a method to compute explicit thermal solutions for laminated and sandwich beams with arbitrary heat source location is developed. The temperature is written as a sum of separated functions of the axial coordinate x, the transverse coordinate z and the volumetric heat source location x_0. The derived non-linear problem implies an iterative process in which three 1D problems are solved successively at each iteration. In the thickness direction, a fourth-order expansion in each layer is considered. For the axial description, classical Finite Element method is used. The presented approach is assessed on various laminated and sandwich beams and comparisons with reference solutions with a fixed heat source location are proposed. Based on the accurate results of the thermal analysis, thermo-mechanical response is also addressed using also a separated representation.

1. Introduction

Composite and sandwich. structures are increasingly used in industrial applications owing to their specific mechanical properties. They can be also submitted to multi-physics environments such as thermal effects, and in particular due to the internal volume heat source. Some applications can be mentioned. In the thermally activated composite (smart material), the deformation of the structure can be controlled by acting on the internal heat source [1]. It requires to know the thermo-mechanical response of the structure for various localized thermal sollicitations. The identification of the damage of composite can be viewed as another illustration. In fact, the determination of the position of the heat source allows some researchers to localize the damaged region, as in [2] for carbon fibre reinforced laminates. In all theses cases, the classical way consists in performing different computations with a fixed value of the heat source position. The present approach based on the variables separation aims at building the explicit thermal solution with respect to this location avoiding the cost of numerous computations. Then, thermo-mechanical analysis can be performed.

In open literature, various mechanical models dedicated to composite or sandwich beams take into account the thermal effects with a fixed value of the heat source location. They can be classified into two families as Equivalent Single Layer (ESL) or Layerwise (LW) models. In the ESL models, the number of unknowns remain low as it is independent of the number of layers. Unfortunately, the physical requirements such as the shear stress continuity at the layer interfaces are not fulfilled. In this family, different types of models can be distinguished: the classical laminate theory [3], the first order shear

* Corresponding author.
E-mail address: philippe.vidal@u-paris10.fr (P. Vidal).

deformation theory ([4] with a linear variation of temperature through the thickness), and higher order theories [5,6] for thermal stresses analysis of beams or plates. The limitations of the ESL approach can be overcome by the LW models. The thermal effect for beam structures has been included in [7]. But, the cost becomes very high as the number of unknowns increases with the number of plies. It should be noted the substantial works developed by Carrera ([8,9]). Various ESL and LW theories with mixed and displacement-based approaches for assumed distribution of temperatures (uniform, linear, localized) are addressed in the framework of the Carrera's Unified Formulation (CUF). Different displacement or stress field approximations over the cross-section are considered. A family of higher-order beam elements can be deduced.

An alternative strategy consists in considering *a priori* physical requirements in the kinematics. Thus, refined models can be built to improve the accuracy of ESL models avoiding the additional computational cost of LW approach. In this way, a zigzag theory for beams has been carried out by Kapuria in [10]. A piecewise linear function along the thickness is used for the temperature. In [11], a global-local approach in conjunction with a Hermite interpolation of the temperature through the thickness is used. For an overview about the thermal analysis, see [5,12–14].

Until now, the so-called Proper Generalized Decomposition (PGD) [15] has shown advantageous characteristics to decrease significatively the computational costs in the framework of the reduction model. Indeed, it allows to decrease the dimensionality of numerous physical problems. For instance, the coordinate variables separation in multi-dimensional PDEs has been performed in [15]. Moreover, this approach has been carried out in [16,17] for mechanical applications involving composite beams and plates. Concerning the thermal analysis, the variables separation of the spatial coordinates x and z has already been used in [18] for laminates. Other parametrized thermal problems have been also considered in [19–21]. Note that the introduction of the load position as a parameter of the solution in the framework of mechanical simulations has been carried out in [22]. For a review about the PGD and its fields of applications, the reader can refer to [23,24].

This work aims at modeling composite beam structures regardless of the volume heat source location for thermo-mechanical analysis. This particular study has not been yet addressed in the previous quoted works. For this purpose, the present approach is based on the separated representation where the temperature is written as a sum of products of unidimensional polynomials of x coordinate, z coordinate, and also the volume thermal heat position x_0. A piecewise fourth-order Lagrange polynomial of z is chosen as it is particularly suitable to model composite structures. As far as the variation with respect to the axial coordinate is concerned, a 1D three-node beam Finite Element (FE) is employed. The functions of the volume heat source position are also piecewise quadratic. Finally, the deduced non-linear problem is linearized. Thus, three 1D linear problems are solved alternatively, in which the number of unknowns is much smaller than in a Layerwise approach. Finally, the solution depends explicitly on the load position.

Then, the thermo-mechanical analysis can be addressed as a weak coupling is considered. The solution of the mechanical problem, also written under a separated form as in [25], is built by considering the temperature distribution as a load. As the separated form of the temperature unknowns are chosen, the nature of the mechanical problem remains unchanged. Moreover, the approach allows us to refine easily the description of the temperature variation without increasing significantly the computational cost which is important to derive an accurate mechanical response.

This article is organized as follows. Firstly, the thermo-mechanical formulation is recalled. The resolution of the parametrized thermal problem based on the variables separation is described. The particular assumption on the temperature field yields a non-linear problem which is solved by an iterative process. Then, the FE discretization is given. Finally, numerical tests are provided. Both thermal loads and thermo-mechanical coupling are considered for laminated and sandwich beams. The behavior of the method is illustrated and discussed. It is assessed by comparing with 2D FEM computations issued from a commercial finite element software with different fixed heat source locations and sizes. The results show the accuracy and the efficiency of the presented method.

2. Thermo-mechanical problem description

A laminated or sandwich beam with *NC* layers is defined in a domain $\mathcal{B} = \mathcal{B}_x \times \mathcal{B}_y \times \mathcal{B}_z = [0, L] \times [-\frac{b}{2} \leq y \leq \frac{b}{2}] \times [-\frac{h}{2} \leq z \leq \frac{h}{2}]$ expressed in a Cartesian coordinate (*x, y, z*). The cross-section of the beam is rectangular. h and b are the height and the width, respectively. The central line of the beam is chosen as the x axis. It is shown in Fig. 1.

In this work, a plane stress assumption is used ($\sigma_{12} = \sigma_{23} = \sigma_{22} = 0$).

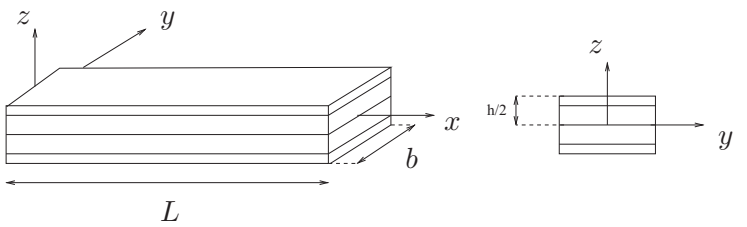

Fig. 1. The laminated beam and co-ordinate system.

2.1. Heat conduction problem

2.1.1. Thermal constitutive equation

Here, the two-dimensional linear heat conduction equations are considered. The constitutive equation is given by the Fourier law

$$\mathbf{Q} = \begin{bmatrix} q_1 \\ q_3 \end{bmatrix} = -\bar{\boldsymbol{\lambda}}\, \mathbf{grad}(\theta), \tag{1}$$

where

$$\bar{\boldsymbol{\lambda}} = \begin{bmatrix} \lambda_1 & 0 \\ 0 & \lambda_3 \end{bmatrix} \text{ and } \mathbf{grad}(\theta) = \begin{bmatrix} \theta_{,x} \\ \theta_{,z} \end{bmatrix}.$$

λ_1, λ_3 are the thermal conductivity components, q_1, q_3 are the heat flux components. They are expressed in the coordinate system x, z. The derivative of the temperature with respect to x and z are denoted $\theta_{,x}$, $\theta_{,z}$, respectively.

2.1.2. The classical weak form of the boundary value problem

For $\delta\theta \in \delta\Theta$ ($\delta\Theta = \{\theta \in H^1(\mathcal{B})/\theta = 0 \text{ on } \partial\mathcal{B}_\theta\}$), the variational principle is given by:
find $\theta \in \Theta$ such that

$$\int\int_{\mathcal{B}} \mathbf{grad}(\delta\theta)^T \mathbf{Q}(\theta)\, d\mathcal{B} + \int\int_{\mathcal{B}} \delta\theta\, r_d\, d\mathcal{B} + \int_{\partial\mathcal{B}_h} \delta\theta\, h_d\, d\partial\mathcal{B} = 0, \quad \forall \delta\theta \in \delta\Theta \tag{2}$$

where r_d and h_d are the prescribed volume heat source and surface heat flux applied on $\partial\mathcal{B}_h$. The temperature θ_d is imposed on $\partial\mathcal{B}_\theta$. Θ is the space of admissible temperatures, i.e. $\Theta = \{\theta \in H^1(\mathcal{B})/\theta = \theta_d \text{ on } \partial\mathcal{B}_\theta\}$.

In the present work, the convection heat transfer and the prescribed surface heat flux are not considered.

2.2. Thermo-mechanical problem

2.2.1. Constitutive relation

The reduced two dimensional constitutive law of the k^{th} layer with thermo-mechanical coupling is given by

$$\boldsymbol{\sigma}^{(k)} = \bar{\mathbf{C}}^{(k)} \left(\boldsymbol{\varepsilon}^{(k)} - \bar{\boldsymbol{\alpha}}^{(k)} \Delta\theta^{(k)} \right), \tag{3}$$

where $\Delta\theta^{(k)} = \theta^{(k)} - \theta_0$ is the variation of temperature.

The stress and strain tensor are supposed to be written as

$$\boldsymbol{\sigma}^T = [\sigma_{11}\ \sigma_{33}\ \tau_{13}], \quad \boldsymbol{\varepsilon}^T = [\varepsilon_{11}\ \varepsilon_{33}\ \gamma_{13}].$$

We have also

$$\bar{\mathbf{C}}^{(k)} = \begin{bmatrix} \bar{C}_{11}^{(k)} & \bar{C}_{13}^{(k)} & 0 \\ & \bar{C}_{33}^{(k)} & 0 \\ symm & & \bar{C}_{55}^{(k)} \end{bmatrix},$$

where $\bar{C}_{ij}^{(k)}$ are the reduced moduli of the material for the k^{th} layer issued from the plane stress assumptions ($\sigma_{22} = 0$). They are given by

$$\bar{C}_{ij}^{(k)} = C_{ij}^{(k)} - C_{i2}^{(k)} C_{j2}^{(k)} / C_{22}^{(k)}. \tag{4}$$

$C_{ij}^{(k)}$ are orthotropic three-dimensional elastic moduli. And, we have $\bar{C}_{55}^{(k)} = C_{55}^{(k)}$.

The vector of the thermal expansion coefficients is $\bar{\boldsymbol{\alpha}}^{(k)^T} = [\alpha_1^{(k)}\ \alpha_3^{(k)}\ 0]$.

2.2.2. The weak form of the boundary value problem

The formulation of the thermo-mechanical problem is written under a displacement-based approach for geometrically linear elastic beams. Using the above notation and Eq. (3), the variational principle is given by:

Find $\mathbf{u}(M) \in U$ such that

$$\int\int_{\mathcal{B}} \delta\boldsymbol{\varepsilon}^T \bar{\mathbf{C}}^{(k)} \boldsymbol{\varepsilon}\ d\mathcal{B} = \int\int_{\partial\mathcal{V}_F} \delta\mathbf{u} \cdot \mathbf{t}\ dS + \int\int_{\mathcal{B}} \delta\boldsymbol{\varepsilon}^T \bar{\mathbf{C}}^{(k)} \bar{\boldsymbol{\alpha}}^{(k)} \Delta\theta\ d\mathcal{B} \quad \forall \delta u \in \delta U, \tag{5}$$

where $\mathbf{t}$ is the prescribed surface forces applied on $\partial\mathcal{V}_F$. U is the space of admissible displacements, i.e. $U = \{\mathbf{u} \in (H^1(\mathcal{B}))^2/\mathbf{u} = \mathbf{u}_d \text{ on } \partial\mathcal{B}_u\}$. We have also $\delta U = \{\mathbf{u} \in (H^1(\mathcal{B}))^2/\mathbf{u} = 0 \text{ on } \partial\mathcal{B}_u\}$. The body forces are not considered in Eq. (5).

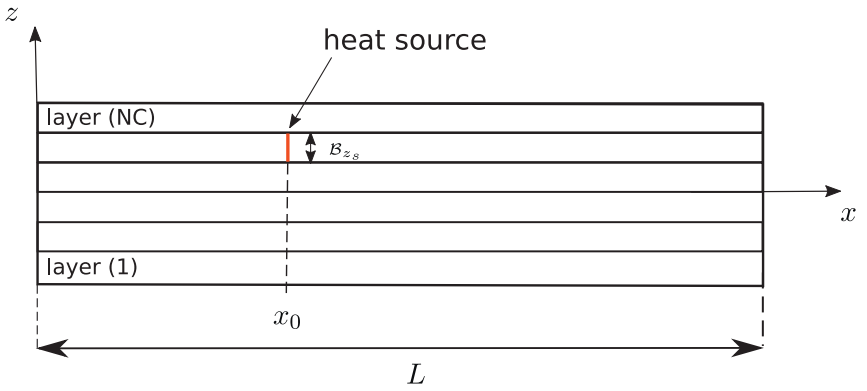

Fig. 2. Volume heat source applied on the laminated beam.

3. Application of the variables separation to the thermal analysis of beam with any volume heat source locations

The Proper Generalized Decomposition (PGD) has been introduced in [15]. It is based on an *a priori* construction of separated variables representation of the solution. In the framework of thermal problems, the solution with separated coordinate variables has been developed in [19]. The following sections are dedicated to the introduction of this approach to build a parametric solution for composite beam submitted to heat sources with any locations. The problem defined by Eqs. (1) and (2) is considered as a parametrized problem where the heat source location x_0 is defined in a bounded interval $[0, L]$. The thermal solution for a point M of coordinate (x, z) of the structure depends on the values of this parameter and is denoted $\theta(x, z, x_0)$ (see Fig. 2).

In the present work, a weak thermo-mechanical coupling is addressed. Once the thermal problem has been solved, the mechanical response is deduced using also the variable separation following [17]. It will not be detailed hereafter for brevity reason. Only the coupling term is detailed in Appendix A.

3.1. The parametrized problem

The temperature solution θ is built as the sum of N products of functions of only one spatial coordinate ($N \in \mathbb{N}$ is the order of the representation) such that:

$$\theta(x, z, x_0) = \sum_{i=1}^{N} f^i(x_0) T_x^i(x) T_z^i(z), \tag{6}$$

where $T_z^i(z)$ is defined on $\mathcal{B}_z$ and $T_x^i(x)$, $f^i(x_0)$ are defined on $\mathcal{B}_x$. A classical quadratic FE approximation is used in $\mathcal{B}_x$ and a LW description is chosen in $\mathcal{B}_z$ as it is particularly suitable for the modeling of composite structures.

The expression of the temperature gradient is written as follows:

$$\mathbf{grad}(\theta) = \sum_{i=1}^{N} f^i(x_0) \begin{bmatrix} T_{x,x}^i(x) T_z^i(z) \\ T_x^i(x) T_{z,z}^i(z) \end{bmatrix}. \tag{7}$$

For a structure submitted to a localized internal heat source at $x = x_0$ in one layer, the parametrized problem can be formulated as:
find $\theta \in \Theta^{ext}$ ($\Theta^{ext} = \{\theta \in H^1(\mathcal{B} \times [0, L]) / \theta = \theta_d \text{ on } \partial\mathcal{B}_\theta \times [0, L]\}$) such that:

$$a(\theta, \delta\theta) = b(\delta\theta), \ \forall \delta\theta \in \delta\Theta^{ext}, \tag{8}$$

with

$$\begin{aligned} a(\theta, \delta\theta) &= -\int_{x_0} \int_{\mathcal{B}} \mathbf{grad}(\delta\theta)^T \mathbf{Q}(\theta) d\mathcal{B} dx_0 \\ b(\delta\theta) &= \int_{x_0} \int_{\mathcal{B}_{z_s}} \delta\theta \, r_d \delta(x - x_0) \, d\mathcal{B}_{z_s} dx_0 \end{aligned} \tag{9}$$

where δ is the Dirac distribution and $\mathcal{B}_{z_s}$ represents the location where the internal heat source is applied (see Fig. 2).

The assumption on the expression of the temperature given in Eq. (6) implies the resolution of a non-linear problem which is described in the following section.

3.2. Resolution of the parametrized problem

A greedy algorithm is used to solve Eq. (8). If we assume that the first m functions (cf. Eq. (6)) have been already computed, the trial function for the iteration $m+1$ can be given by

$$\theta^{m+1}(x,z,x_0) = \theta^m(x,z,x_0) + f(x_0)T_x(x)T_z(z), \tag{10}$$

where f, T_x and T_z are the unknown functions and θ^m is the associated known sets at iteration m defined by

$$\theta^m(x,z,x_0) = \sum_{i=1}^{m} f^i(x_0)T_x^i(x)T_z^i(z). \tag{11}$$

The problem to be solved given in Eq. (8) can be written as

$$a(f\,T_x\,T_z, \delta\theta) = b(\delta\theta) - a(\theta^m, \delta\theta). \tag{12}$$

The test function is

$$\delta(f\,T_x\,T_z) = \delta f\,T_x\,T_z + f\,\delta T_x\,T_z + f\,T_x\,\delta T_z. \tag{13}$$

Introducing the test function defined by Eq. (13) and the trial function defined by Eq. (10) into the weak form Eq. (12) leads to the three following problems:

- for the test function δT_x

$$a(f\,T_z\,T_x, f\,T_z\,\delta T_x) = b(f\,T_z\,\delta T_x) - a(\theta^m, f\,T_z\,\delta T_x),\ \forall \delta T_x, \tag{14}$$

- for the test function δT_z

$$a(f\,T_x\,T_z, f\,T_x\,\delta T_z) = b(f\,T_x\,\delta T_z) - a(\theta^m, f\,T_x\,\delta T_z),\ \forall \delta T_z, \tag{15}$$

- for the test function δf

$$a(T_x\,T_z\,f, T_x\,T_z\,\delta f) = b(T_x\,T_z\,\delta f) - a(\theta^m, T_x\,T_z\,\delta f),\ \forall \delta f. \tag{16}$$

From Eqs. (14)–16, a coupled non-linear problem to be solved is deduced. Classically, a fixed point method is carried out for simplicity reason. Starting from an initial function $\tilde{T}_x^{(0)}$, $\tilde{T}_z^{(0)}$, $\tilde{f}^{(0)}$, we construct a sequence $\tilde{T}_x^{(k)}$, $\tilde{T}_z^{(k)}$ and $\tilde{f}^{(k)}$ which satisfy Eqs. 14–16, respectively. For each problem, only one unknown 1D function has to be found, the two other ones are assumed to be known (from the previous step of the fixed point strategy). So, the approach leads to the process given in Algorithm 1.

Algorithm 1 Present algorithm.

for $n = 1$ to N_{max} **do**
  Initialize $\tilde{T}_x^{(0)}$, $\tilde{T}_z^{(0)}$, $\tilde{f}^{(0)}$
  for $k = 1$ to k_{max} **do**
    Compute $\tilde{f}^{(k)}$ from Eq. (16) (straightforward resolution), $\tilde{T}_x^{(k-1)}$, $\tilde{T}_z^{(k-1)}$ being known
    Compute $\tilde{T}_z^{(k)}$ from Eq. (15) (linear equation on $\mathcal{B}_z$), $\tilde{f}^{(k)}$ and $\tilde{T}_x^{(k-1)}$ being known
    Compute $\tilde{T}_x^{(k)}$ from Eq. (14) (linear equation on $\mathcal{B}_x$), $\tilde{f}^{(k)}$ and $\tilde{T}_z^{(k)}$ being known
    Check for convergence
  end for
  Set $f^{n+1} = \tilde{f}^{(k)}$, $T_z^{n+1} = \tilde{T}_z^{(k)}$, $T_x^{n+1} = \tilde{T}_x^{(k)}$
  Set $\theta^{n+1} = \theta^n + f^{n+1}\,T_z^{n+1}\,T_x^{n+1}$
  Check for convergence
end for

The fixed point algorithm is stopped when

$$\frac{\| f^{(k+1)}T_x^{(k+1)}T_z^{(k+1)} - f^{(k)}T_x^{(k)}T_z^{(k)} \|_{\mathcal{B}\times\mathcal{B}_x}}{\| f^{(0)}T_x^{(0)}T_z^{(0)} \|_{\mathcal{B}\times\mathcal{B}_x}} \leq \varepsilon, \tag{17}$$

where $\|A\|_{\mathcal{B}\times\mathcal{B}_x} = \left[\int_{\mathcal{B}_x}\int_{\mathcal{B}_z}\int_{\mathcal{B}_x} A^2\,dx\,dz\,dx_0\right]^{1/2}$ and ε is a small parameter to be fixed by the user. In the present study, we set $\varepsilon = 10^{-6}$.

3.3. FE discretization

To solve the beam problem previously introduced, a discrete representation of the functions (T_x, T_z) is chosen. A classical finite element approximation in $\mathcal{B}_x$ and $\mathcal{B}_z$ is used. The elementary vectors of degree of freedom (dof) associated with the finite element mesh in $\mathcal{B}_x$ and $\mathcal{B}_z$ are denoted $\mathbf{q}_e^x$ and $\mathbf{q}_e^z$, respectively. The temperature fields and the associated gradient are computed from the values of $\mathbf{q}_e^x$ and $\mathbf{q}_e^z$ by

$$\begin{aligned} T_{xe} &= \mathbf{N}_x \mathbf{q}_e^x, \qquad \mathcal{E}_x^e = \mathbf{B}_x \mathbf{q}_e^x, \\ T_{ze} &= \mathbf{N}_z \mathbf{q}_e^z, \qquad \mathcal{E}_z^e = \mathbf{B}_z \mathbf{q}_e^z, \end{aligned} \tag{18}$$

where $\mathcal{E}_x^{eT} = [T_{x,x} \quad T_x]$ and $\mathcal{E}_z^{eT} = [T_z \quad T_{z,z}]$. The matrices $[\mathbf{N}_x]$, $[\mathbf{B}_x]$, $[\mathbf{N}_z]$, $[\mathbf{B}_z]$ contain the interpolation functions, their derivatives and the jacobian components. They are built following the chosen discrete representation.

3.4. Finite element problem to be solved on $\mathcal{B}_x$

For the sake of simplicity, the functions $\tilde{f}^{(k)}$ and $\tilde{T}_z^{(k)}$ which are assumed to be known, will be denoted $\tilde{f}$ and $\tilde{T}_z$, and the function $\tilde{T}_x^{(k)}$ to be computed will be denoted T_x. The gradient in Eq. (14) can be written as

$$\mathbf{grad}(\tilde{T}_z T_x) = \mathbf{\Sigma_z}(\tilde{T}_z)\mathcal{E}_x, \tag{19}$$

with

$$\mathbf{\Sigma_z}(\tilde{T}_z) = \begin{bmatrix} \tilde{T}_z & 0 \\ 0 & \tilde{T}_{z,z} \end{bmatrix}. \tag{20}$$

The variational problem defined on $\mathcal{B}_x$ from Eq. (14) is

$$\int_{\mathcal{B}_x} \delta\mathcal{E}_x^T \boldsymbol{\lambda}_{x_0 z}(\tilde{f}, \tilde{T}_z)\mathcal{E}_x dx = r_d Q_{z_s}(\tilde{T}_z) \int_{\mathcal{B}_x} \tilde{f}\delta T_x dx - \int_{\mathcal{B}_x} \delta\mathcal{E}_x^T \mathbf{Q}_{x_0 z}(\tilde{f}, \tilde{T}_z, \theta^m) dx, \tag{21}$$

with

$$\boldsymbol{\lambda}_{x_0 z}(\tilde{f}, \tilde{T}_z) = \int_{\mathcal{B}_x} \tilde{f}^2 \, dx_0 \int_{\mathcal{B}_z} \mathbf{\Sigma_z}(\tilde{T}_z)^T \, \bar{\boldsymbol{\lambda}} \, \mathbf{\Sigma_z}(\tilde{T}_z) dz, \tag{22}$$

$$\mathbf{Q}_{x_0 z}(\tilde{f}, \tilde{T}_z, \theta^m) = \int_{\mathcal{B}_x} \int_{\mathcal{B}_z} \tilde{f} \, \mathbf{\Sigma_z}(\tilde{T}_z)^T \, \bar{\boldsymbol{\lambda}} \, \mathbf{grad}(\theta^m) dz \, dx_0, \tag{23}$$

$$Q_{z_s}(\tilde{T}_z) = \int_{\mathcal{B}_{z_s}} \tilde{T}_z dz, \tag{24}$$

r_d is considered as constant.

Note that Eq. (23) can split into two independent integrals over $\mathcal{B}_x$ and $\mathcal{B}_z$ as θ^m is written under a separated form.

The introduction of the finite element approximation Eq. (18) in the variational Eq. (21) allows us to deduce the following linear system:

$$\boldsymbol{\Lambda}_{x_0 z}(\tilde{f}, \tilde{T}_z) \, \mathbf{q}^x = \mathcal{R}_x(\tilde{f}, \tilde{T}_z, \theta^m), \tag{25}$$

where $\mathbf{q}^x$ is the nodal temperatures vector associated with the FE mesh in $\mathcal{B}_x$, $\boldsymbol{\Lambda}_{x_0 z}(\tilde{f}, \tilde{T}_z)$ the conductivity matrix obtained by summing the elements' conductivity matrices $\boldsymbol{\Lambda}_{x_0 z}^e(\tilde{f}, \tilde{T}_z)$ and $\mathcal{R}_x(\tilde{f}, \tilde{T}_z, \theta^m)$ the equilibrium residual obtained by summing the elements' residual load vectors $\mathcal{R}_x^e(\tilde{f}, \tilde{T}_z, \theta^m)$

$$\boldsymbol{\Lambda}_{x_0 z}^e(\tilde{f}, \tilde{T}_z) = \int_{L_e} \mathbf{B}_x^T \, \boldsymbol{\lambda}_{x_0 z}(\tilde{f}, \tilde{T}_z) \, \mathbf{B}_x dx \tag{26}$$

and

$$\mathcal{R}_x^e(\tilde{f}, \tilde{T}_z, \theta^m) = r_d Q_s(\tilde{T}_z) \int_{L_e} \mathbf{N}_x^T \tilde{f} \, dx - \int_{L_e} \mathbf{B}_x^T \mathbf{Q}_{x_0 z}(\tilde{f}, \tilde{T}_z, \theta^m) dx. \tag{27}$$

L_e refers to one element of the mesh in $\mathcal{B}_x$ ($\mathcal{B}_x = \cup L_e$).

3.5. Finite element problem to be solved on $\mathcal{B}_z$

For simplicity reason as in the previous section, the functions $\tilde{f}^{(k)}$ and $\tilde{T}_x^{(k-1)}$ which is assumed to be known, will be denoted $\tilde{f}$, $\tilde{T}_x$, and the unknown function $\tilde{T}_z^{(k)}$ will be denoted T_z. The gradient in Eq. (15) becomes

$$\mathbf{grad}(\tilde{T}_x T_z) = \mathbf{\Sigma_x}(\tilde{T}_x)\mathcal{E}_z \tag{28}$$

with

$$\mathbf{\Sigma_x}(\tilde{T}_x) = \begin{bmatrix} \tilde{T}_{x,x} & 0 \\ 0 & \tilde{T}_x \end{bmatrix}. \tag{29}$$

The variational problem defined on $\mathcal{B}_z$ from Eq. (15) is

$$\int_{\mathcal{B}_z} \delta\mathcal{E}_z^T \boldsymbol{\lambda}_{x_0x}(\tilde{f},\tilde{T}_x)\mathcal{E}_z dx = r_d\, Q_{x_0x_s}(\tilde{f},\tilde{T}_x) \int_{\mathcal{B}_{z_s}} \delta T_z dz - \int_{\mathcal{B}_z} \delta\mathcal{E}_z^T \mathbf{Q}_{x_0x}(\tilde{f},\tilde{T}_x,\theta^m) dx \tag{30}$$

with

$$\boldsymbol{\lambda}_{x_0x}(\tilde{f},\tilde{T}_x) = \int_{\mathcal{B}_x} \tilde{f}^2\, dx_0 \int_{\mathcal{B}_x} \mathbf{\Sigma_x}(\tilde{T}_x)^T\, \bar{\boldsymbol{\lambda}}\, \mathbf{\Sigma_x}(\tilde{T}_x) dx, \tag{31}$$

$$\mathbf{Q}_{x_0x}(\tilde{f},\tilde{T}_x,\theta^m) = \int_{\mathcal{B}_x}\int_{\mathcal{B}_x} \tilde{f}\, \mathbf{\Sigma_x}(\tilde{T}_x)^T\, \bar{\boldsymbol{\lambda}}\, \mathbf{grad}(\theta^m) dx\, dx_0, \tag{32}$$

$$Q_{x_0x_s}(\tilde{f},\tilde{T}_x) = \int_{\mathcal{B}_x} \tilde{f}\,\tilde{T}_x\, dx. \tag{33}$$

As in Eq. (23), the integral in Eq. (32) can split for the same reason.
The introduction of the finite element discretization Eq. (18) in the variational Eq. (30) leads to the linear system

$$\boldsymbol{\Lambda}_{x_0x}(\tilde{f},\tilde{T}_x)\,\mathbf{q}^z = \mathcal{R}_z(\tilde{f},\tilde{T}_x,\theta^m), \tag{34}$$

where $\mathbf{q}^z$ is the nodal temperature vector associated with the FE mesh in $\mathcal{B}_z$, $\boldsymbol{\Lambda}_{x_0x}(\tilde{f},\tilde{T}_x)$ the conductivity matrix obtained by summing the elements' conductivity matrices $\boldsymbol{\Lambda}^e_{x_0x}(\tilde{f},\tilde{T}_x)$ and $\mathcal{R}_z(\tilde{f},\tilde{T}_x,\theta^m)$ the equilibrium residual obtained by summing the elements' residual load vectors $\mathcal{R}^e_z(\tilde{f},\tilde{T}_x,\theta^m)$

$$\boldsymbol{\Lambda}^e_{x_0x}(\tilde{f},\tilde{T}_x) = \int_{Lz_e} \mathbf{B}_z^T\, \boldsymbol{\lambda}_{x_0x}(\tilde{f},\tilde{T}_x)\, \mathbf{B}_z dz \tag{35}$$

and

$$\mathcal{R}^e_z(\tilde{f},\tilde{T}_x,\theta^m) = r_d\, Q_{x_0x_s}(\tilde{f},\tilde{T}_x) \int_{Lz_e^{source}} \mathbf{N}_z^T dz - \int_{Lz_e} \mathbf{B}_z^T \mathbf{Q}_{x_0x}(\tilde{f},\tilde{T}_x,\theta^m) dz. \tag{36}$$

Lz_e refers to one element of the mesh in $\mathcal{B}_z$ ($\mathcal{B}_z = \cup Lz_e$).

3.6. Determination of f on $\mathcal{B}_x$

As previously, the known functions $\tilde{T}_x^{(k-1)}$, $\tilde{T}_z^{(k-1)}$ and the unknown function $\tilde{f}^{(k)}$ are denoted $\tilde{T}_x$, $\tilde{T}_z$ and f, respectively. The introduction of the separated form Eq. (10) in Eq. (16) allows us to deduce the straightforward relation:

$$\left[\int_{\mathcal{B}} \mathbf{grad}(\tilde{T}_z\tilde{T}_x)^T\, \bar{\boldsymbol{\lambda}}\, \mathbf{grad}(\tilde{T}_z\tilde{T}_x) d\mathcal{B}\right] f = r_d \tilde{T}_x \int_{\mathcal{B}_{z_s}} \tilde{T}_z dz - \int_{\mathcal{B}} \mathbf{grad}(\tilde{T}_z\tilde{T}_x)^T\, \bar{\boldsymbol{\lambda}}\, \mathbf{grad}(\theta^m) d\mathcal{B}. \tag{37}$$

Remark: For a volume heat source applied on a given region denoted I_s, the calculation of the temperature is carried out following two steps. First, the computation of the functions f^i, T_x^i and T_z^i in Eq. (6) is performed. Second, only a integration over I_s of the terms f^i in the explicit solution is computed at the post-processing level.

4. Numerical results: thermal analysis

In this section, the following FE discretization is chosen: (i) a classical 3-node quadratic FE for the thermal unknowns depending on the x-axis coordinate, (ii) a classical quadratic interpolation for the function f, (iii) a fourth-order layer-wise description for the transverse direction.

Static thermal tests are presented evaluating the efficiency and the properties of the algorithm and also validating our approach. To this purpose, a sandwich test is addressed. The convergence of the method, the influence of the location and size of the thermal load are discussed. The approach is assessed by comparing with 2D FEM solutions using a commercial code. Finally, the separated variables decomposition is compared with a common tensor decomposition to illustrate the performance of the method.

4.1. Localized volumetric heat source on the upper face of a sandwich beam

A sandwich beam, given in [10], submitted to a localized heat source on the upper face is considered. The test is described as follows:

geometry: A three-layer sandwich beam with graphite-epoxy faces and a soft core with thickness $e = 0.1h$ is considered. $S = \dfrac{L}{h} = 10$.

boundary conditions: localized volumetric heat source over $[xs^{(1)}_{min}, xs^{(1)}_{max}]$ in the upper face of the sandwich with a constant value $r_d = 0.1$ W.m^{-3}
zero temperature on the bottom surface of the beam such as $\theta(x, z = -h/2) = 0$

material properties: The orientation of all the plies is $\gamma_k = 0,\ k = 1, 2, 3$.
for the face: $\lambda_L = 1.5$ W.m^{-1}.K^{-1}, $\lambda_T = 0.5$ W.m^{-1}.K^{-1}
where L refers to the fiber direction, T refers to the transverse direction.
for the core: isotropic material such as $\lambda = 3.0$ W.m^{-1}.K^{-1}

mesh: $N_x = 60$ (number of elements along the whole beam)

results: For a fixed heat source location, 2D FEM computations using Ansys with a very refined mesh of PLANE25 elements is provided (120 elements along the length and 70 elements along the thickness). Results based on the variables separation x and z, denoted VS-LD4, are also provided. These results are considered as reference solutions.

4.1.1. heat source for three locations

First, the approach is assessed for three different locations of the heat source over $I_1 = [0, 10]$, $I_2 = [10, 20]$ and $I_3 = [40, 50]$. For a thermal load over I_i, three error indicators between a reference solution θ^{ref} (VS-LD4) and a separated variables solution θ^n of order n is introduced:

1. energy error indicator

$$\epsilon_n = 100\sqrt{\frac{a_{err}(\theta^n - \theta^{ref}, \theta^n - \theta^{ref})}{a_{err}(\theta^{ref}, \theta^{ref})}}$$
$$\text{with } a_{err}(\theta_1, \theta_2) = \int_{\mathcal{B}_x}\int_{\mathcal{B}_z} \mathbf{grad}(\theta_1)^T \bar{\boldsymbol{\lambda}}\, \mathbf{grad}(\theta_2)\ \ dz\, dx, \tag{38}$$

2. global error indicator

$$\epsilon_n^{\square} = 100\sqrt{\frac{\displaystyle\int_{\mathcal{B}_x}\int_{\mathcal{B}_z} (\square^n - \square^{ref})^2\ \ dz\, dx}{\displaystyle\int_{\mathcal{B}_x}\int_{\mathcal{B}_z} \square^{ref^2}\ \ dz\, dx}}, \tag{39}$$

where $\square$ stands for θ, q_1 and q_3

3. error indicator on the maximum value

$$\epsilon_n^{\theta_{max}} = 100\sqrt{\frac{(\theta^n_{max} - \theta^{ref}_{max})^2}{\theta^{ref\,2}_{max}}}, \tag{40}$$

The variation of the energy error indicator Eq. (38) with respect to the number of triplets (T^i_x, T^i_z, f^i) is represented on Fig. 3 for the three locations of the heat source. The trend of these three configurations is rather similar. The obtained curve can be divided into two parts with two different slopes, the first one being over 0 to 15 triplets, and the second

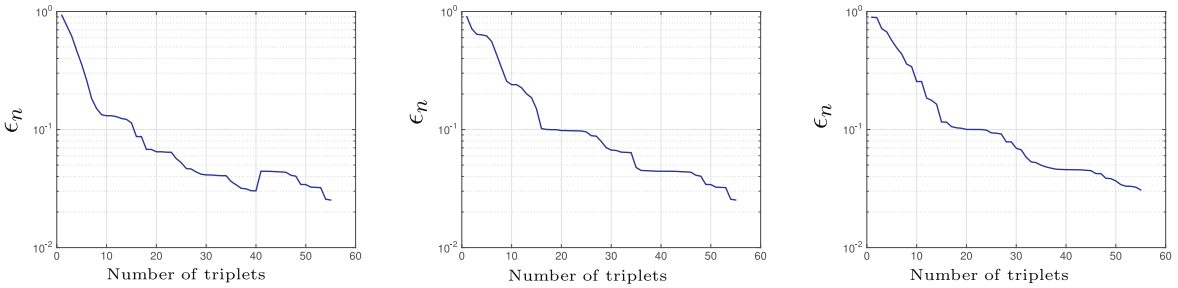

(a) $I_1 = [0, 10]$ (b) $I_2 = [10, 20]$ (c) $I_3 = [40, 50]$

Fig. 3. Energy error indicator with respect to the number of triplets for three locations of volume heat source.

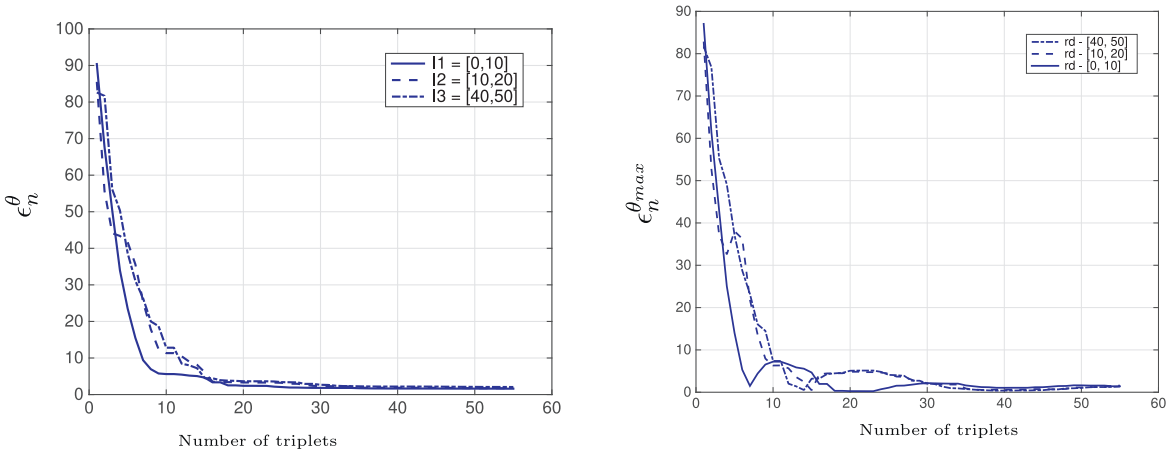

Fig. 4. Global error indicator (left) - θ_{max} error indicator (right) for three locations of volume heat source.

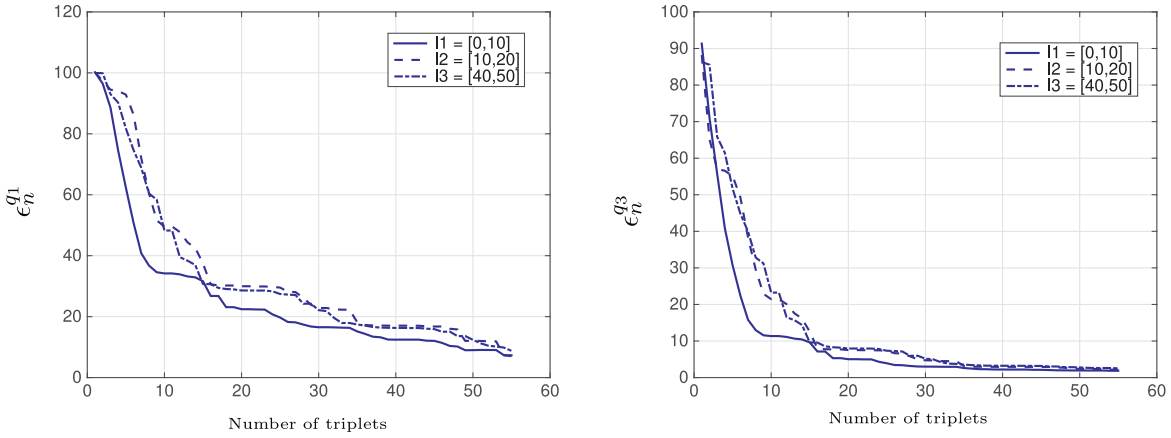

Fig. 5. Global error indicator q_1(left) - q_3 (right) for three locations of volume heat source.

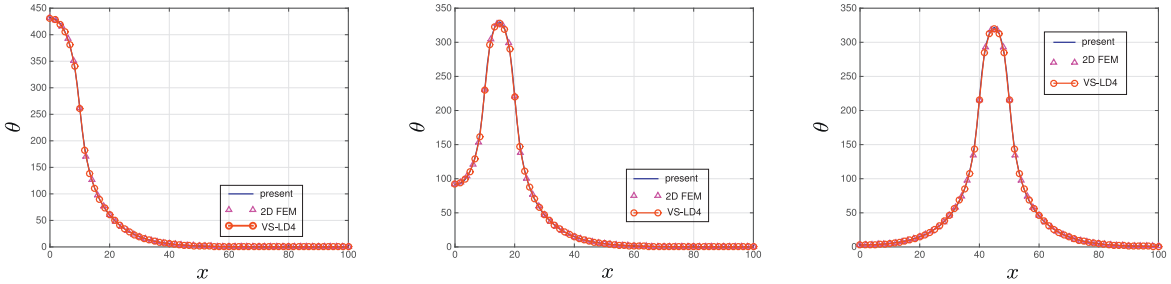

(a) $I_1 = [0, 10]$ (b) $I_2 = [10, 20]$ (c) $I_3 = [40, 50]$

Fig. 6. Distribution of the temperature along the beam axis for 3 locations of volume heat source at $x = (xs_{min}^{(1)} + xs_{max}^{(1)})/2$ - 50 triplets.

one beyond 15 triplets. For further investigations, Fig. 4 shows the error rate on the global and maximum temperatures versus the number of terms for the different cases. Again, we can notice that the error rate is greatly reduced with only 15 couples, then the new couples do not bring any significant corrections. Nevertheless, as it can be highlighted in Fig. 5, the axial heat flux q_1 is the most difficult quantity to obtain with accuracy, and additional terms are needed to improve the estimation of q_1. 50 triplets are needed to have an error rate of less than 1%, whereas 40 triplets are sufficient for the maximum temperature with the same level of error.

To illustrate the accuracy of the approach, the distributions of temperature along the axis and the thickness of the beam, and the variation of the transverse heat flux for three locations of the heat source are shown in Figs. 6–8, respectively. It can be inferred from these figures that the parametrized approach is in very good agreement with the 2D reference solution

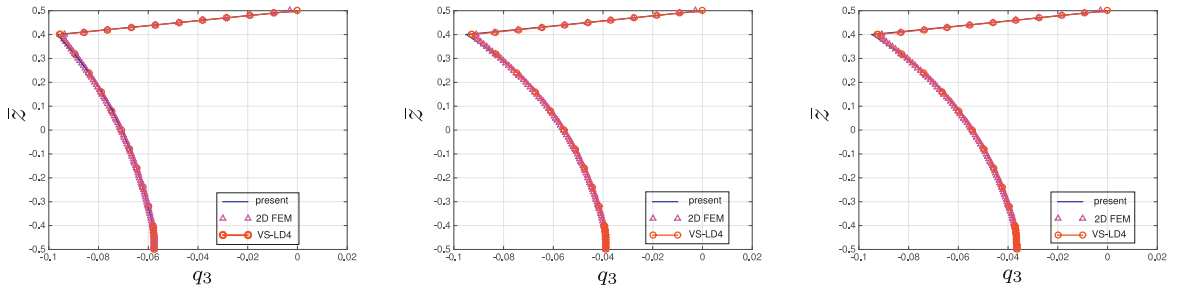

(a) $I_1 = [0, 10]$ (b) $I_2 = [10, 20]$ (c) $I_3 = [40, 50]$

Fig. 7. Distribution of the transverse heat flux along the thickness for 3 locations of volume heat source at $x = (xs^{(1)}_{min} + xs^{(1)}_{max})/2$ - 50 triplets.

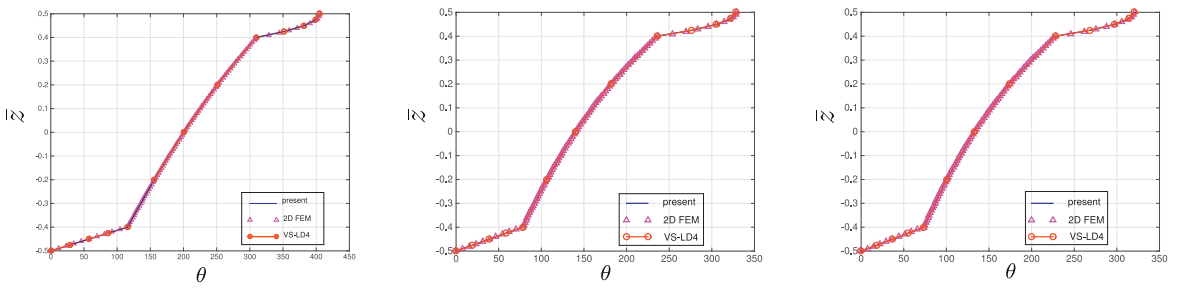

(a) $I_1 = [0, 10]$ (b) $I_2 = [10, 20]$ (c) $I_3 = [40, 50]$

Fig. 8. Distribution of the temperature across the thickness for 3 locations of volume heat source - 50 triplets.

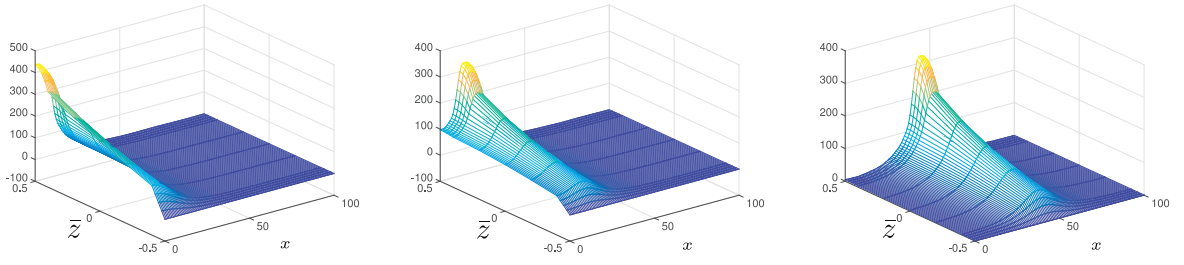

(a) $I_1 = [0, 10]$ (b) $I_2 = [10, 20]$ (c) $I_3 = [40, 50]$

Fig. 9. Distribution of the temperature for 3 locations of volume heat source - 50 triplets.

computed with ANSYS regardless of the position of the volumetric thermal load, from the edge to the middle of the structure. The localized temperature rise is well-captured (see Figs. 6 and 9). As far as the transverse heat flux is concerned, the free boundary condition on the top of the beam and the continuity condition at the layers interface are fullfiled (cf. Fig. 7). The high variation in the upper layer is also well-represented. Finally, it can be noticed that the separated representation approach (x and z coordinates), denoted VS-LD4, with a fixed location of heat source leads to very accurate results, and could be considered as a reference solution.

4.1.2. Influence of the size of the heat source region

To further assess the method, localized volume heat source over a very small region is considered with three locations ($I^L_1 = [0, 5/3]$, $I^L_2 = [10, 35/3]$, $I^L_3 = [40, 125/3]$). The variation of the error rate is shown in Fig. 10. It can be inferred from this figure that the convergence rate is slower than the previous case as it could be expected. Indeed, this load case implies a high variation of the temperature along the beam axis around the heat source region as it can be seen in Fig. 11. 34 couples are needed to obtain a global error rate $\epsilon^\theta_n < 1\%$. Nevertheless, 55 couples are required to obtain the maximal temperature with accuracy (about 2%) due to the localization effect on the distribution. For illustration, the fifty first triplets T^i_x, T^i_z and f^i are given in Figs. 12–14. The variations of T^i_x and f^i are rather similar. These results were expected considering Eq. (37) because they have shorter wavelengths when the number of the triplet increases. For the function T^i_z, the variation along the thickness (Fig. 13) seems to be identical beyond the 10th one. Nevertheless, it is not the case as heat flux are corrected by these additional terms.

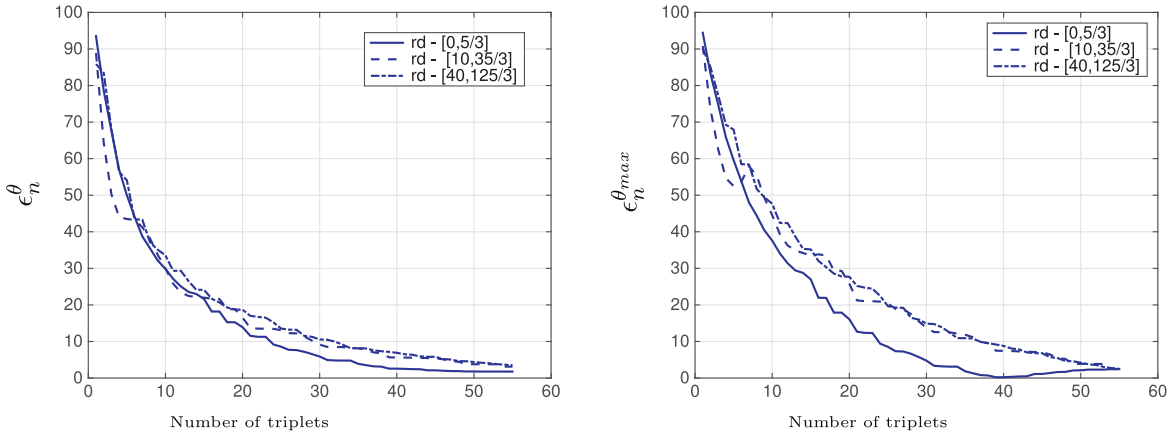

Fig. 10. Global error rate (left) - θ_{max} error rate (right) for three very localized regions of volume heat source (I_1^L, I_2^L, I_3^L).

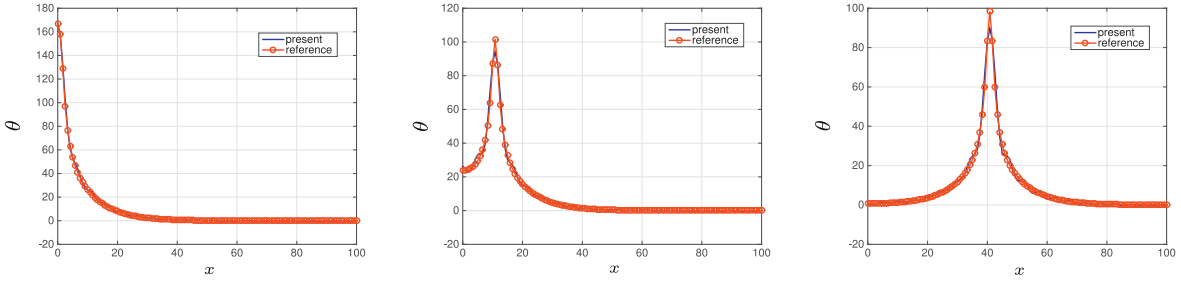

(a) $I_1^L = [0, 5/3]$ (b) $I_2^L = [10, 35/3]$ (c) $I_3^L = [40, 125/3]$

Fig. 11. Distribution of the temperature along the beam axis for 3 locations of volume heat source - 55 triplets.

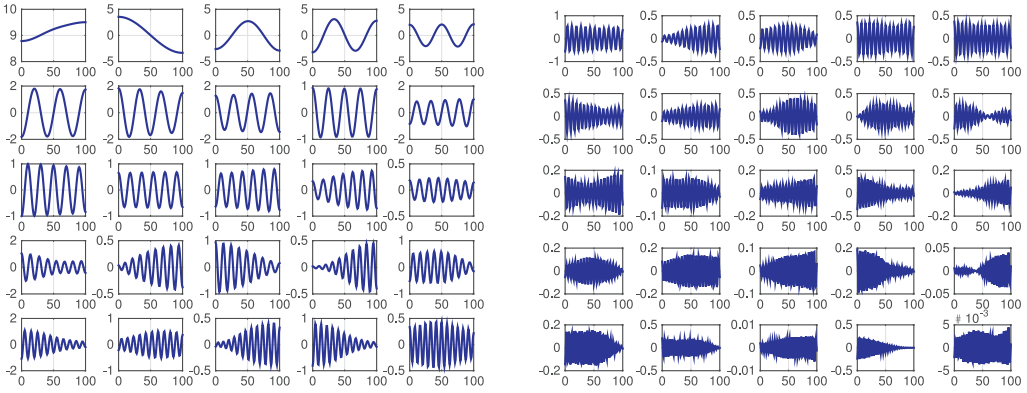

Fig. 12. $T_x^i(x)$.

Finally, it can be concluded that the accuracy of the method is very good when compared with the reference solution.

4.2. Comparison with CANDECOMP - PARAFAC approach

To evaluate the efficiency of the decomposition algorithm developed in the previous section, the results are compared with the canonical decomposition and parallel factor (CANDECOMP - PARAFAC, denoted HOSVD-PC) [26,27] which is a common tensor decomposition. For that, an estimate of the best rank-R Candecomp Parafac model of a tensor X is computed using an alternating least-squares (ALS) algorithm available in [28]. The process consists in factorizing a given N^{th} order tensor $\boldsymbol{X}$ into a sum of component rank-one tensors (set of N component matrices $\boldsymbol{A}^n$ with $\boldsymbol{A}^n = [\boldsymbol{a}_1^n, \ldots, \boldsymbol{a}_R^n]$, $\boldsymbol{A}^n \in \mathbb{R}^{I_n \times R}$,

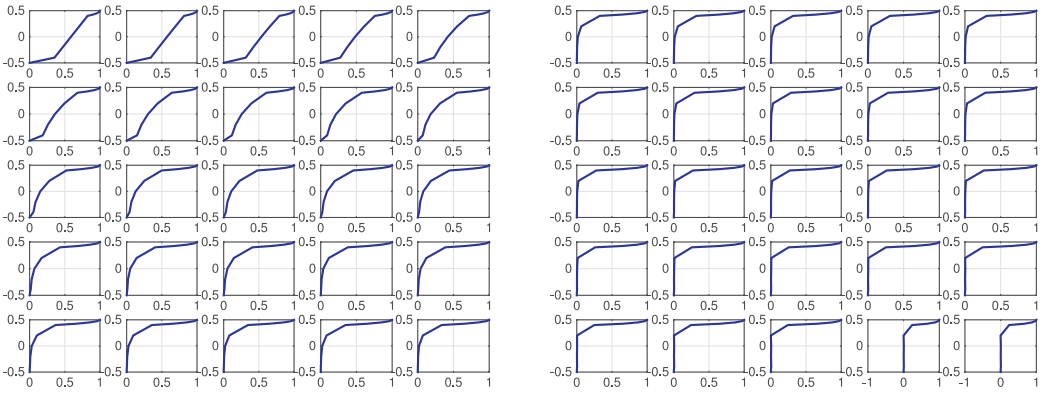

Fig. 13. $T_z^i(z)$.

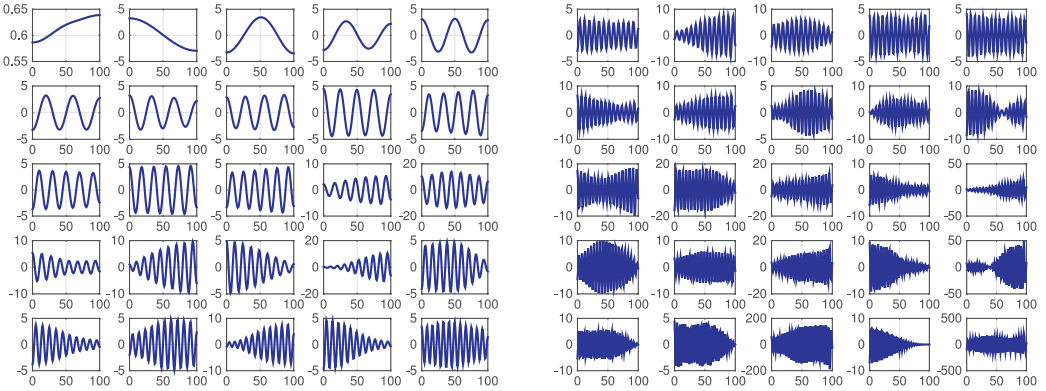

Fig. 14. $f^i(x_0)$.

$(n = 1, \ldots, N))$ that is

$$\boldsymbol{X} \approx \sum_{r=1}^{R} \boldsymbol{a}_r^1 \circ \boldsymbol{a}_r^2 \ldots \boldsymbol{a}_r^N = \widehat{\boldsymbol{X}} \text{ such that } \min_{\widehat{\boldsymbol{X}}} \|\boldsymbol{X} - \widehat{\boldsymbol{X}}\|_F^2$$

where $\|\|_F$ is the Frobenius norm and "$\circ$" denotes outer product.

In our case, we have $N = 3$ and $\boldsymbol{a}_r^1$, $\boldsymbol{a}_r^2$, $\boldsymbol{a}_r^3$ corresponds to T_x^r, T_z^r, f^r respectively. The tensor $\widehat{\boldsymbol{X}}$ is computed using the solution $\boldsymbol{X}$ obtained with 55 triplets. The test involves a volume heat source applied on only the size of one element ($xs \in [40, 125/3]$, namely 1.6% of the length of the beam). To compare with the present approach, two types of error rate, a global one Eq. (39) and a local one Eq. (40), are given in Fig. 15. It can be observed that the results are rather similar. It shows the performance of the present decomposition process.

Then, the energy contribution of each triplet to the total solution is also compared in Fig. 16. For the present approach, 55% and 87% of the total energy are included in the first 8 and 25 triplets, respectively. The figure illustrates well the behavior of the greedy type algorithm. On the contrary, for the HOSVD-PC approach, it is important to notice that the decomposition provided for a given number of terms cannot be truncated. This number must be chosen *a priori*. We see clearly that there is no hierarchy in the different terms of the summation (see Fig. 16 right), which is a drawback. In fact, to obtain this figure, it is needed to compute all the terms each time for a fixed value of R.

5. Numerical results: thermo-mechanical analysis

The numerical method described in [17] to solve the mechanical problem is used as it has shown interesting features in terms of accuracy and efficiency. Again, a fourth-order expansion for the z-functions is considered. As the present study is restricted to a weak thermo-mechanical coupling, once the thermal problem is solved following the presented approach, the resolution of the mechanical one is limited to the computation of the second term of the right hand side of Eq. (5). It is important to note that this integral can be also divided into 2 parts, one over $\mathcal{B}_x$ and the other one over $\mathcal{B}_z$ as the temperature is written under a separated form. Thus, the key point of the method remains available. This computation is given in Appendix A.

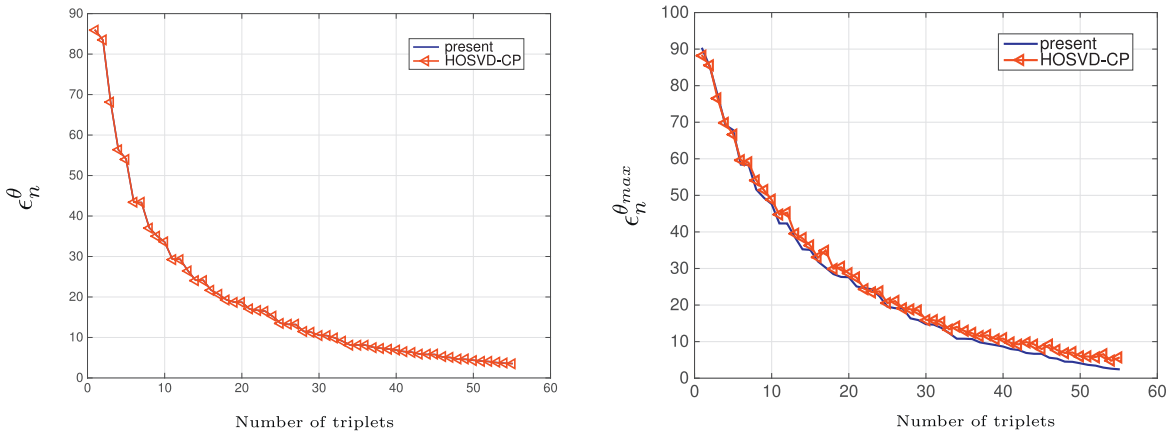

Fig. 15. global error rate (left) - θ_{max} error rate (right) - comparison between present approach and HOSVD-PC.

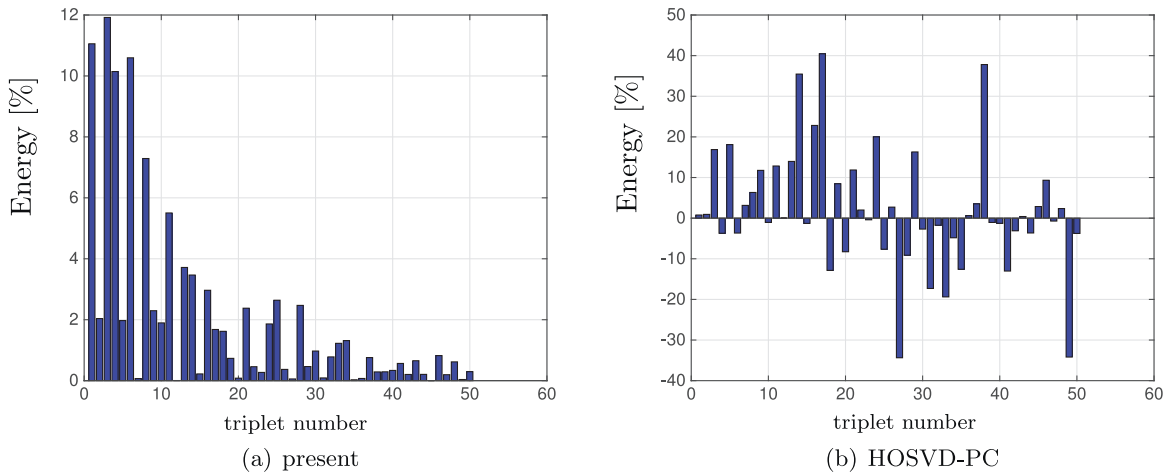

Fig. 16. Contribution of each triplet in the total energy [%].

In this section, a 8-layer cross-ply beam is considered. The test case is described as follows:

geometry: composite cross-ply beam [0°/90°/0°/90°/0°/90°/0°/90°] with $S = 5$ and $L = 100$. The thickness of each layer ($h/8$) is the same.
boundary conditions:

- *Thermal load*: prescribed temperature such as $\theta(0, z) = 0$ and $\theta(x, -h/2) = 0$, and internal volume heat sources in the 4^{th} layer
- *Mechanical BC*: simply-supported beam

material properties: $E_L = 181$ GPa, $E_T = 10.3$ GPa, $G_{LT} = 7.17$ GPa, $G_{TT} = 2.87$ GPa, $\nu_{LT} = 0.28$, $\nu_{TT} = 0.33$, $\alpha_L = 0.02\ 10^{-6}\ \mathrm{K}^{-1}$, $\alpha_T = 22.5\ 10^{-6}\ \mathrm{K}^{-1}$,
$\lambda_L = 1.5\ \mathrm{W.m}^{-1}.\mathrm{K}^{-1}$, $\lambda_T = 0.5\ \mathrm{W.m}^{-1}.\mathrm{K}^{-1}$
mesh: the whole beam is meshed, $N_x = 100$.
results: The results $(\bar{\sigma}_{11}, \bar{\sigma}_{13})$ are nondimensionalized using: $\bar{\sigma}_{11} = \dfrac{\sigma_{11}}{\alpha_T E_T \theta_0} \bar{\sigma}_{13} = \dfrac{S\sigma_{13}}{\alpha_T E_T \theta_0}$, with $\theta_0 = 10$, $\bar{z} = z/h$. The results are compared with 2D FEM analysis using Ansys with plane stress assumptions and converged mesh from the previous section. The eight-node element PLANE77 is used for the thermal part and PLANE183 for the mechanical analysis.

5.1. Thermal results with any volume heat source locations

The distribution of the 25 unknown functions in Eq. (6) is shown in Fig. 17. The variation of the functions T_z^i which depends on the z coordinate shows the importance of the LayerWise description of the temperature through the thickness. The thermal load implies a localized temperature rise that is difficult to represent with a equivalent single layer approach.

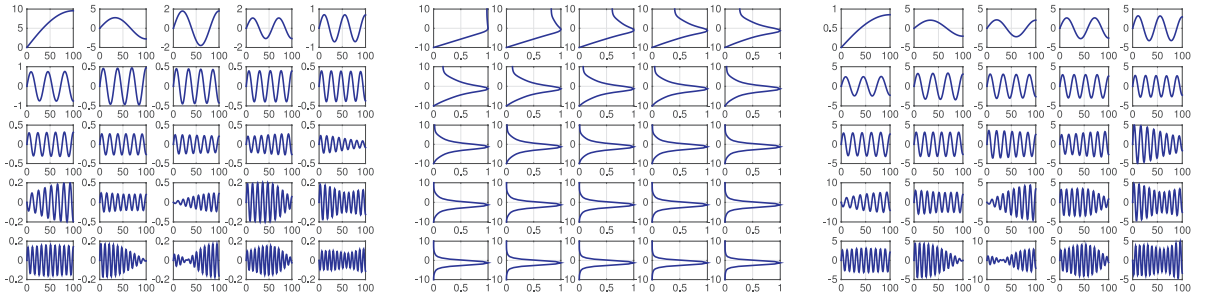

Fig. 17. $T_x^i(x)$ (left), $T_z^i(z)$ (middle), $f^i(x_0)$ (right).

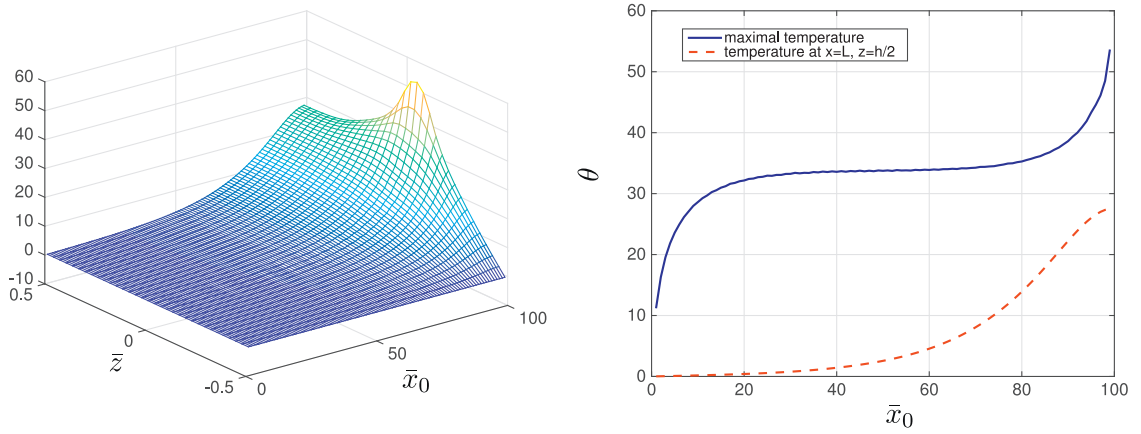

Fig. 18. Distribution of the temperature with respect to the position of the heat source $\bar{x}_0$ (right) and also along the thickness at $x = L$ (left) - 8 layers.

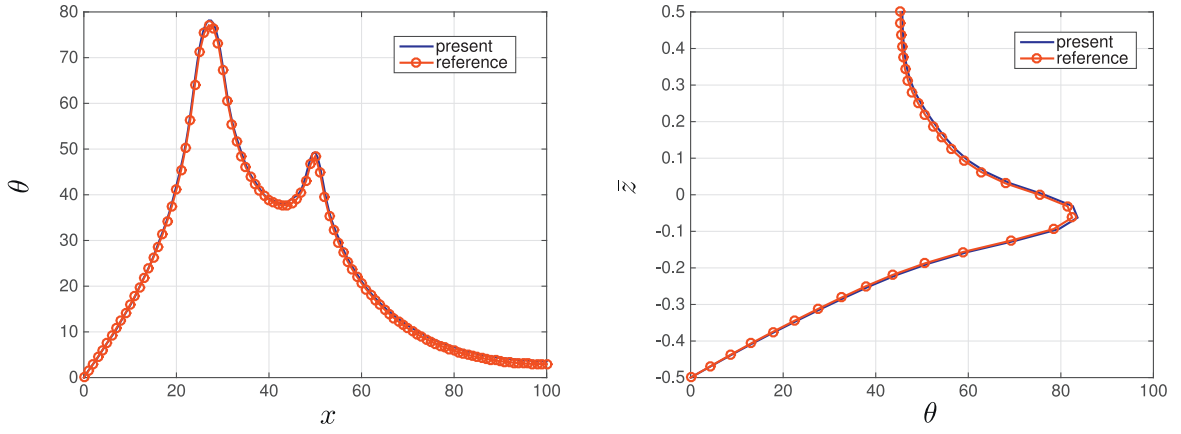

Fig. 19. Distribution of the temperature along the length of the beam at $z = 0$ (left) and along the thickness at the middle of the interval I_1^{4th} (right) -8 layers.

To illustrate the possibility of the method, a volume heat source over $[\bar{x}_0 - \Delta, \bar{x}_0 + \Delta]$ with $\Delta = L/N_x$ is considered. The temperature variation with respect to the position of the heat source $\bar{x}_0$ is shown in Fig. 18. The distribution of the temperature through the thickness at the end of the beam, the maximal temperature and the temperature at $z = h/2$, $x = L$ are provided. In a classical approach, 100 computations with a fixed heat source location are required to plot these curves. On the contrary, for the present method, the influence of the position of the thermal load is quantified in a straightforward manner. The maximal temperature is influenced by the boundary conditions at the edges of the beam (Fig. 18 (right)). Obviously, the level of temperature at the end of the beam increases when the heat source is close to this one, but the relation is not linear (Fig. 18 right - dotted line).

To assess the results, two heat sources localized in the 4th layer over the region $I_1^{4\text{th}} = [24, 30]$ and $I_2^{4\text{th}} = [49, 51]$, with an intensity $r_d^{(1)} = 0.8$ and $r_d^{(2)} = 1$ are considered. We can see that the temperature and the heat flux are in very good agreement with the reference solution (cf Figs. 19 and 20). The influence of the two heat sources on the temperature varia-

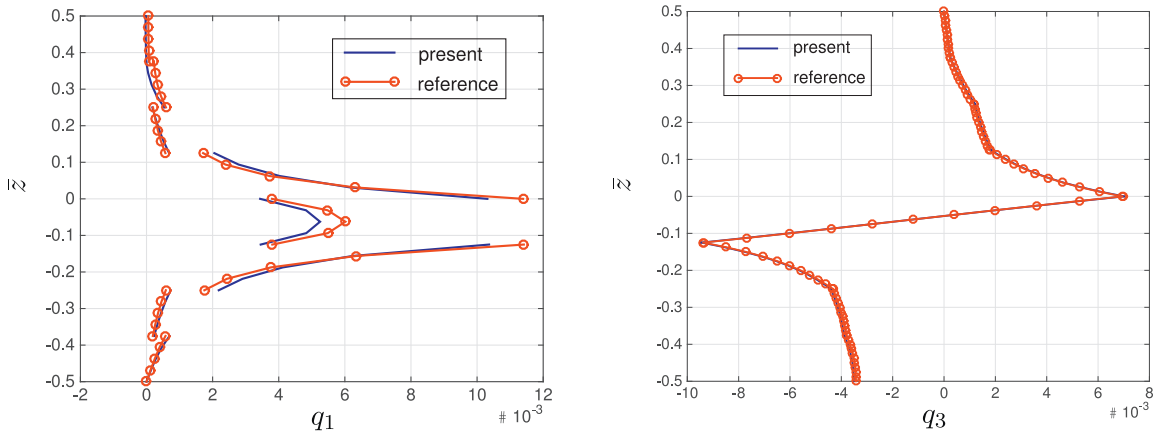

Fig. 20. Distribution of heat flux q_1 at $x = 30$ (left) and q_3 at the middle of the interval $I_1^{4^{th}}$ (right) along the thickness - 8 layers.

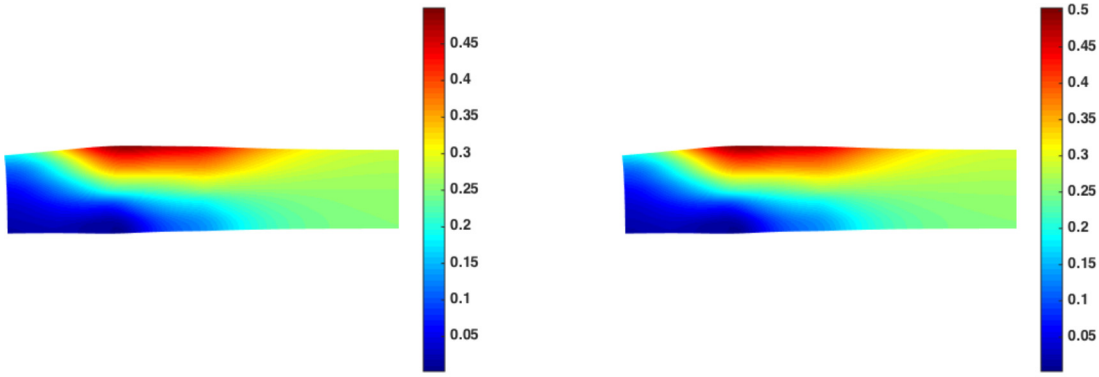

(a) present (b) Ansys

Fig. 21. Distribution of displacement - scale factor = 5 - 8 layers - 10 couples.

tion is clearly visible along the axis beam (Fig. 19 left), and also across the thickness (Fig. 19 right). Again, the temperature rise is well captured. The complex distribution of q_1 and q_3 with respect to z coordinate is also well represented. Finally, the explicit solution allows us to consider any number of heat source with any location and intensity very easily without additional computational cost.

5.2. Mechanical response

Once the thermal analysis is solved considering the test case of the previous section, the mechanical response is computed using the separated representation on the spatial coordinates x and z. The accuracy of the temperature distribution over the whole beam, and in particular through the thickness is important to predict the mechanical response with accuracy. In fact, it has been emphasized the localized influence of the thermal source on the corresponding results.

For the presented test case, 10 couples are needed to build the solution. First, the 2D deformed shape of the beam is shown in Fig. 21 and compared with the reference solution from Ansys computation. The norm of the displacement is given. The structure is submitted to bending and stretching in the thickness direction. To illustrate the possibility of the approach to provide 2D results, the distribution of the axial and transverse shear stress are given in Figs. 22 and 23. The accuracy of the results are excellent when compared with the reference solution, despite the high localization effect inside the structure. In fact, a strong gradient occurs in the vicinity of the thermal load (two regions), and it is well represented by the present method. Moreover, the two different intensities of the internal sources induce very different stresses levels in these regions. It can be clearly seen for the transverse shear stress in Fig. 23. For such analysis, a LayerWise description is required to capture this gradient. Finally, the distribution of the maximal stresses $(\bar{\sigma}_{11}, \bar{\sigma}_{13})$ through the thickness is given in Fig. 24. Whereas it is rather complex, the accuracy of the results is very satisfactory.

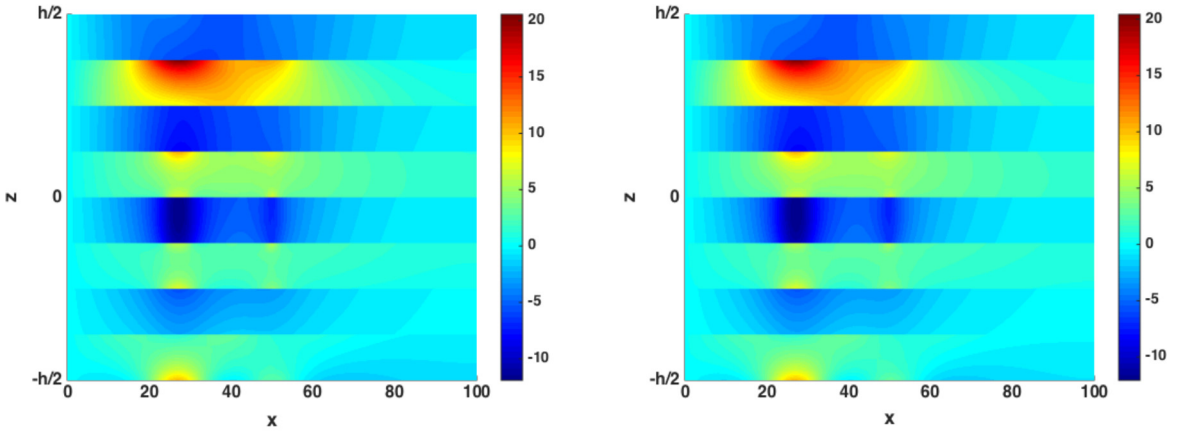

(a) present (b) Ansys

Fig. 22. Distribution of $\bar{\sigma}_{11}$ (different scale for x and z-axis) - 8 layers - 10 couples.

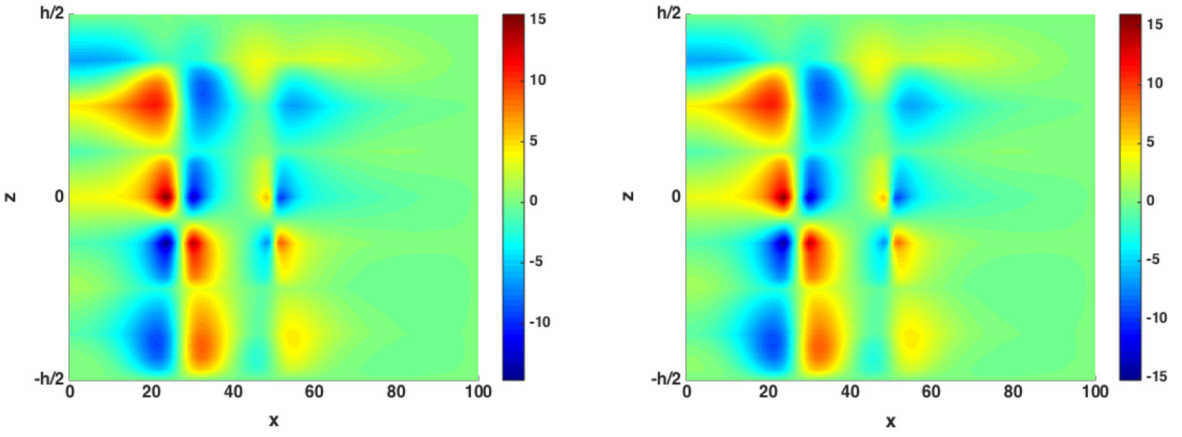

(a) present (b) Ansys

Fig. 23. Distribution of $\bar{\sigma}_{13}$ (different scale for x and z-axis) - 8 layers - 10 couples.

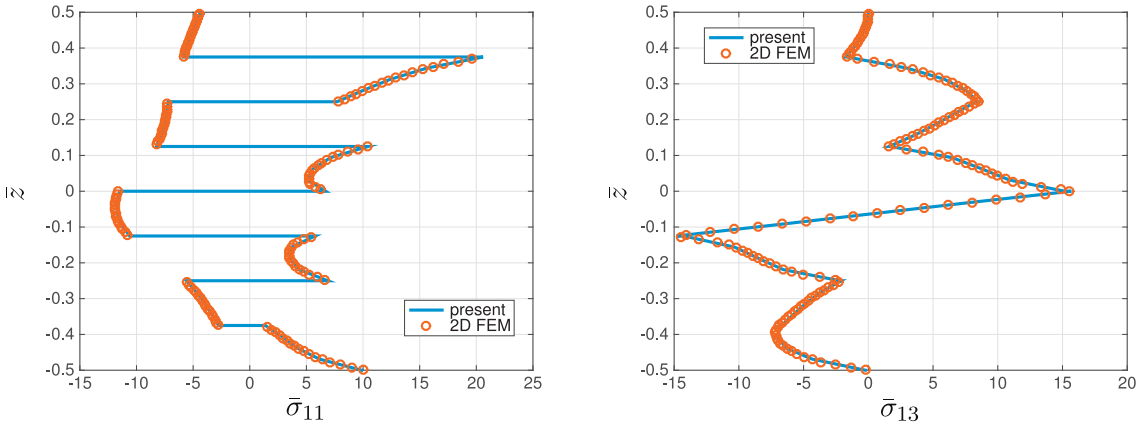

Fig. 24. Distribution of $\bar{\sigma}_{11}$ at $x = 28$ (left) and $\bar{\sigma}_{13}$ at $x = 24$ (right) along the thickness - S=10 - 8 layers - 10 couples.

6. Conclusion

In the present study, an explicit thermal solution with respect to the volume heat source location has been built for laminated composite and sandwich beams. For this purpose, the temperature is expressed as a separated representation of three 1D functions (coordinates x / z, and heat source location x_0). Thus, the deduced iterative algorithm needs the resolution of only 1D problems and each of them implies a low computational cost. The total cost depends on the number of triplets built to represent the solution.

The behavior of the approach is illustrated on various benchmarks. The performance of the decomposition process of the solution is also shown. The method is assessed by comparing with reference solutions, and the results are very satisfactory. The distribution of the thermal quantities is rather complex, and the high-order expansion of the temperature through the thickness is particularly suitable to represent that with accuracy. Then, from these accurate results, the thermo-mechanical coupling has been addressed. For such thermal loads, a refined description of the mechanical quantity is needed to capture the localization effect occurring in the thickness of the structure. For that, a LayerWise approach coupled with a variables separation appears to be a very attractive method to predict stresses with accuracy. The computational cost is much lower than classical LW approach or 3D computations.

Moreover, the solution allows us to study directly the influence of the heat source location without any additional computational cost, because it does not require the computations of many configurations with some fixed thermal loads. Once the explicit thermal solution is built, all the subsequent responses can be immediately deduced. So, the approach can be advantageously used for parametric problems such as identification, inverse problems, reliability ...

Appendix A. Thermo-mechanical load

The procedure to compute the second term of the right hand side of Eq. (5) is described here. It is denoted $I_{thme} = \int\int_{\mathcal{B}} \delta\boldsymbol{\epsilon}^T \tilde{\mathbf{C}}^{(k)} \tilde{\boldsymbol{\alpha}}^{(k)} \Delta\theta \; dV$. In the following, the notations defined in [17] are used. We recall that the displacement is written under a separated form as

$$\mathbf{u}(x,z) = \sum_{i=1}^{N_{mech}} \mathbf{f}^i(z) \circ \mathbf{v}^i(x) + \mathbf{f}(z) \circ \mathbf{v}(x), \tag{A.1}$$

where $\mathbf{f}$ and $\mathbf{v}$ are the unknown functions to be determined.

Thus, two problems have to be solved. We can express the strain as follows:

$$\varepsilon(\tilde{\mathbf{f}} \circ \mathbf{v}) = \mathbf{B}_z(\tilde{f})\mathcal{E}_v \;\text{ with }\; \mathcal{E}_v = \mathbf{B}_x^{mech}\mathbf{q}^v \tag{A.2}$$

and

$$\varepsilon(\tilde{\mathbf{v}} \circ \mathbf{f}) = \mathbf{B}_x(\tilde{v})\mathcal{E}_f \;\text{ with }\; \mathcal{E}_f = \mathbf{B}_z^{mech}\mathbf{q}^f. \tag{A.3}$$

The matrices $\mathbf{B}_x^{mech}$ and $\mathbf{B}_z^{mech}$ contain the interpolation functions, their derivatives and the jacobian components dependent on the chosen discrete representation. The vector of dofs associated with the FE mesh in $\mathcal{B}_x$ and $\mathcal{B}_z$ is denoted $\mathbf{q}^v$ and $\mathbf{q}^f$, respectively. The notation $\sim$ refers to a known function.

A.1. FE problem to be solved on $\mathcal{B}_x$

Using Eq. (A.2) and the expression of the temperature under the separated form given in Eq. (6), I_{thme} can be expressed under the following form:

$$I_{thme} = \int_{\mathcal{B}_x} \delta\mathcal{E}_v^T \sum_{i=1}^{N} f^i(x_0) \underbrace{\int_{\mathcal{B}_z} \mathbf{B}_z^T(\bar{f})\bar{\mathbf{C}}^{(k)}\bar{\boldsymbol{\alpha}}^{(k)} T_z^i(z)\, dz}_{\mathbf{f}^i_{thme_z}} \; T_x^i(x)\, dx \tag{A.4}$$

Thus, the elements' thermo-mechanical load is written as

$$\mathbf{F}^e_{thme_z}(\bar{f}) = \sum_{i=1}^{N} f^i(x_0) \int_{L_e} \mathbf{B}_x^{mech^T} \mathbf{f}^i_{thme_z} T_x^i(x)\, dx. \tag{A.5}$$

A.2. FE problem to be solved on $\mathcal{B}_z$

Using Eqs. (A.3) and (6), we can deduce that

$$I_{thme} = \int_{\mathcal{B}_z} \delta\mathcal{E}_f^T \sum_{i=1}^{N} f^i(x_0) \underbrace{\int_{\mathcal{B}_x} \mathbf{B}_x^T(\bar{v})\bar{\mathbf{C}}^{(k)}\bar{\boldsymbol{\alpha}}^{(k)} T_x^i(x)\, dx}_{\mathbf{f}^{(k)^i}_{thme_x}} \; T_z^i(z)\, dz \tag{A.6}$$

Thus, the elements' thermo-mechanical load is deduced:

$$\mathbf{F}^{e}_{thme_x}(\tilde{v}) = \sum_{i=1}^{N} f^{i}(x_0) \int_{z_e} \mathbf{B}_z^{mech^T} \mathbf{f}^{(k)^i}_{thme_x} T_z^i(z)\, dz. \tag{A.7}$$

Thus, the computation of I_{thme} split into two integrations over $\mathcal{B}_x$ and $\mathcal{B}_z$.

References

[1] H. Drobez, G.L. OHostis, K.B. Gautier, F. Laurent, B. Durand, A new active composite, Smart Mater. Struct. 18 (2) (2009) 025020.
[2] V. Munoz, B. Valès, M. Perrin, M. Pastor, H. Welemane, A. Cantarel, M. Karama, Damage detection in CFRP by coupling acoustic emission and infrared thermography, Compos. Part B Eng. J. 85 (2016) 68–75.
[3] Y. Tanigawa, H. Murakami, Y. Ootao, Transient thermal stress analysis of a laminated composite beam., J. Thermal Stress. 12 (1989) 25–39.
[4] G. Blandford, T. Tauchert, Y. Du, Self-strained piezothermoelastic composite beam analysis using first-order shear deformation theory, Compos. Part B Eng. J. 30 (1) (1999) 51–63.
[5] J. Reddy, Mechanics of Laminated Composite Plates–Theory and Analysis., CRC Press, Boca Raton, FL, 1997.
[6] P. Vidal, O. Polit, A thermomechanical finite element for the analysis of rectangular laminated beams., Finite Elem. Anal. Des. 42 (10) (2006) 868–883, doi:10.3166/reef.11.379-392.
[7] H.-J. Lee, D. Saravanos, Coupled layerwise analysis of thermopiezoelectric composite beams, AIAA J. 34 (6) (1996) 1231–1237.
[8] E. Carrera, An assessment of mixed and classical theories for the thermal stress analysis of orthotropic multilayered plates., J. Thermal Stress. 23 (2000) 797–831.
[9] E. Carrera, A. Ciuffreda, Closed-form solutions to assess multilayered-plate theories for various thermal stress problems., J. Thermal Stress. 27 (2004) 1001–1031.
[10] S. Kapuria, P. Dumir, A. Ahmed, An efficient higher order zigzag theory for composite and sandwich beams subjected to thermal loading., Int. J. Solids Struct. 40 (2003) 6613–6631.
[11] M. Lezgy-Nazargah, Fully coupled thermo-mechanical analysis of bi-directional FGM beams using NURBS isogeometric finite element approach., Aerosp. Sci. Tech. 45 (2015) 154–164.
[12] R. Hetnarski, M. Eslami, Thermal Stresses - Advanced Theory and Applications., Springer, 2009.
[13] T. Tauchert, Thermally induced flexure, buckling and vibration of plates., Appl. Mech. Rev. 44 (8) (1991) 347–360.
[14] A. Noor, W. Burton, Computational models for high-temperature multilayered composite plates and shells., Appl. Mech. Rev. 45 (10) (1992) 419–446.
[15] A. Ammar, B. Mokdada, F. Chinesta, R. Keunings, A new family of solvers for some classes of multidimensional partial differential equations encountered in kinetic theory modeling of complex fluids, J. Non Newton. Fluid Mech. 139 (2006) 153–176.
[16] B. Bognet, F. Bordeu, F. Chinesta, A. Leygue, A. Poitou, Advanced simulation of models defined in plate geometries: 3D solutions with 2D computational complexity., Comput. Methods Appl. Mech. Eng. 201–204 (2012) 1–12, doi:10.1016/j.cma.2011.08.025.
[17] P. Vidal, L. Gallimard, O. Polit, Assessment of a composite beam finite element based on the proper generalized decomposition., Compos. Struct. 94 (5) (2012) 1900–1910, doi:10.1016/j.compstruct.2011.12.016.
[18] P. Vidal, L. Gallimard, O. Polit, Thermo-mechanical analysis of laminated composite and sandwich beams based on a variables separation., Compos. Struct. 152 (2016) 755–766, doi:10.1016/j.compstruct.2016.05.082.
[19] E. Pruliere, F. Chinesta, A. Ammar, A. Leygue, A. Poitou, On the solution of the heat equation in very thin tapes., Int. J. Thermal Sci 65 (2013) 148–157.
[20] C. Ghnatios, F. Masson, A. Huerta, A. Leygue, E. Cueto, F. Chinesta, Proper generalized decomposition based dynamic data-driven control of thermal processes., Comput. Methods Appl. Mech. Eng. 213–216 (2012) 29–41.
[21] J. Aguado, A. Huerta, F. Chinesta, E. Cueto, Real-time monitoring of thermal processes by reduced-order modeling., Int. J. Num. Meth. Eng. 102 (5) (2015) 991–1017.
[22] S. Niroomandi, I. Alfaro, E. Cueto, F. Chinesta, Model order reduction for hyperelastic materials, Int. J. Num. Meth. Eng. 81 (9) (2010) 1180.
[23] A. Nouy, A priori model reduction through proper generalized decomposition for solving time-dependent partial differential equations, Comput. Methods Appl. Mech. Eng. 199 (23–24) (2010) 1603–1626.
[24] F. Chinesta, A. Ammar, A. Leygue, R. Keunings, An overview of the proper generalized decomposition with applications in computational rheology, J. Non- Newton. Fluid Mech. 166 (11) (2011) 578–592.
[25] P. Vidal, L. Gallimard, O. Polit, Proper generalized decomposition and layer-wise approach for the modeling of composite plate structures., Int. J. Solids Struct. 50 (14–15) (2013) 2239–2250, doi:10.1016/j.ijsolstr.2013.03.034.
[26] R.A. Harshman, Foundations of the parafac procedure: Models and conditions for an explanatory multi-modal factor analysis., UCLA Work. Pap. Phon. 16 (1970) 1–84.
[27] A.L. Kiers, Towards a standardized notation and terminology in multiway analysis., J. Chemom. 14 (2000) 105–122.
[28] B.W. Bader, T.G.y Kolda, et al., http://www.sandia.gov/tgkolda/TensorToolbox/Matlab tensor toolbox version 2.6, Available online (February 2015). http://www.sandia.gov/tgkolda/TensorToolbox/.